ROYAL SOCIETY OF CHEMISTRY

Check for updates

The first lead cobalt phosphite, PbCo$_2$(HPO$_3$)$_3$†

Vadim M. Kovrugin, [ID] *[a,b,c] Marie Colmont, [ID] [a] Oleg I. Siidra, [ID] [b]
Sergey V. Krivovichev, [ID] [b] Silviu Colis[d] and Olivier Mentré [ID] *[a]

Single crystals of a new lead cobalt phosphite, PbCo$_2$(HPO$_3$)$_3$, have been synthesized using mild hydro-thermal techniques and characterized by X-ray diffraction analysis, SQUID magnetic measurements, IR spectroscopy, UV/vis spectroscopy, thermogravimetric analysis, and scanning electron microscopy. PbCo$_2$(HPO$_3$)$_3$ crystallizes in the non-centrosymmetric (NCS) $R3m$ space group, a = 5.3145(15) Å, c = 25.494(7) Å, V = 623.6(4) Å^3. The crystal structure of PbCo$_2$(HPO$_3$)$_3$ is based upon 2D heteropolyhedral blocks built up from Co$_2$O$_9$ octahedral dimers and HPO$_3$ pseudo-tetrahedra. Lead cations reside in the interlayer space of the structure. Here, the NCS character results reasonably from the cooperative Pb^{2+} lone electron pair arrangements, by analogy to the centrosymmetric compound (NH$_4$)$_2$Co$_2$(HPO$_3$)$_3$ with similar but disordered blocks. A local twisting of specific HPO$_3$ groups arises due to unreasonably short H···H contacts between two phosphite oxoanions. In terms of the magnetic behavior, the new PbCo$_2$(HPO$_3$)$_3$ phase demonstrates weak antiferromagnetic interactions inside the Co$_2$O$_9$ dimers between cobalt ions as expected from the phosphite μ-O bridges.

1. Introduction

Nowadays, interest in transition metal phosphites is focused mainly on hybrid organic/inorganic compounds since they favor the formation of microporous materials with open-framework zeolite-type structures, which may find various applications in ion-exchange, separation, and catalysis.[1–3] Dealing with "pure" inorganic chemistry, the specific intrinsic bonding scheme of phosphite [HPO$_3$]$^{2-}$ groups and tridentate ligand species offer other interesting possibilities to achieve original topologies between transition metals, compared to common tetradentate phosphate [PO$_4$]$^{3-}$ groups. Both having tetrahedral geometry, they exhibit a similar structural chemistry, but with important differences due to the smaller charge within an asymmetric charge distribution in [HPO$_3$]$^{2-}$. For instance, it was demonstrated that the pseudo-tetrahedral phosphite oxoanions can

replace the phosphate groups in novel open crystal structures as reported for zinc phosphites.[4,5] Also note that the strongly covalent P–H bond in HPO$_3$ negatively polarizes the H$^{\delta-}$ corner. Thus, it plays a role analogous to that of the lone electron pair E in specific oxoanions such as ESe^{4+}O$_3$, as demonstrated by the recent report on Fe$_2$(SeO$_3$)$_3$ *versus* Fe$_2$(HPO$_3$)$_3$.[6] The co-presence of asymmetric anionic groups and stereochemically active lone electron pairs of cations (*e.g.* Sn^{2+}, Pb^{2+}, Sb^{3+}, Bi^{3+}) in solids appears as a promising route to non-centrosymmetric polar crystal structures,[7–10] very attractive in terms of their possible applications in optics, asymmetric catalysis and enantioselective separation processes.[11,12] The Co-containing systems are an important group of this kind of materials mainly owing to their ability to achieve various coordination environments (tetrahedral, bipyramidal, and octahedral) and versatile valence states. The Co-containing compositions combined with organic ligands can also be used for the preparation of metal–organic frameworks with higher surface areas, higher porosity, and various atomic arrangements.[13] Moreover, the Co-containing materials based on HPO$_3$ anionic groups may exhibit particular magnetic[14,15] or photosensitive properties.[16,17] Particularly, due to the weak aptitude of phosphite as magnetic transmitters,[6,14] they can form ideal diamagnetic spacers. Despite the report of about twenty different hybrid organic/inorganic cobalt phosphite phases, the structural chemistry of inorganic cobalt phosphites remains poorly explored. There are only a few reported cobalt phosphites, namely, NaCo(H$_2$PO$_3$)$_3$(H$_2$O),[18] Co(HPO$_3$)(H$_2$O),[19] Co$_{11}$(HPO$_3$)$_8$(OH)$_6$,[20] and Na$_2$Co(HPO$_3$)$_2$.[21] In order to

aUnité de Catalyse et Chimie du Solide (UCCS), UMR 8181 CNRS, Université Lille 1 Sciences et Technologies, 59655 Villeneuve d'ASCQ, France. E-mail: kovrugin_vm@hotmail.com, olivier.mentre@ensc-lille.fr
bDepartment of Crystallography, Institute of Earth Sciences, St. Petersburg State University, 199034 St. Petersburg, Russian Federation
cLaboratoire de Réactivité et Chimie des Solides (LRCS), UMR 7314 CNRS, Université de Picardie Jules Verne, 80039 Amiens Cedex, France
dInstitut de Physique et Chimie des Matériaux de Strasbourg (IPCMS), UMR 7504 UDS-CNRS (UDS-ECPM), 67034 Cedex 2 Strasbourg, France
†Electronic supplementary information (ESI) available. See DOI: 10.1039/c7dt02279d

fill up the gap in the structural chemistry of inorganic cobalt-based phosphites, we report on the synthesis, structural characterization, and magnetic properties of the first cobalt phosphite containing lead, *i.e.*, $PbCo_2(HPO_3)_3$ which turns out to be non-centrosymmetric, as expected.

2. Experimental

2.1 Synthesis

Commercial PbO (crystalline powder, 99.9% Aldrich), Co_3O_4 (crystalline powder, 95%, Alfa Aesar), and H_3PO_3 (crystalline powder, 98%, Acros Organics) were used as received.

The title compound has been prepared under mild hydrothermal conditions. The main reasons for choosing the method based on crystallization from aqueous solutions are the high hygroscopicity of phosphorous acid (H_3PO_3), and its decomposition into phosphoric acid (H_3PO_4) and phosphine (PH_3) at a relatively low temperature around 200 °C. Although several attempts were made to obtain a pure polycrystalline sample by combining the stoichiometric amounts of starting reactants, secondary phases always accompanied the title compound (Table 1). To grow single crystals of the novel $PbCo_2(HPO_3)_3$ composition suitable for the X-ray diffraction analysis, a mixture of PbO (0.1488 g, 0.67 mmol), Co_3O_4 (0.0803 g, 0.33 mmol), and H_3PO_3 (0.1639 g, 2.0 mmol) was dissolved in 6 ml of distilled water. The hydrothermal reaction was performed in a 23 ml Teflon-lined steel autoclave heated to 160 °C in a mechanical convection oven. The temperature of the oven was held constant for two days, followed by slow cooling to room temperature for 48 hours. Pink pseudo-hexagonal prismatic blocks (Fig. 1a and b) of the title compound were observed in association with transparent platy crystals of $PbHPO_4$.[22,23] The crystals of the $PbCo_2(HPO_3)_3$ compound were carefully washed with ethanol to remove the unwanted admixture of $PbHPO_4$ and then dried in air.
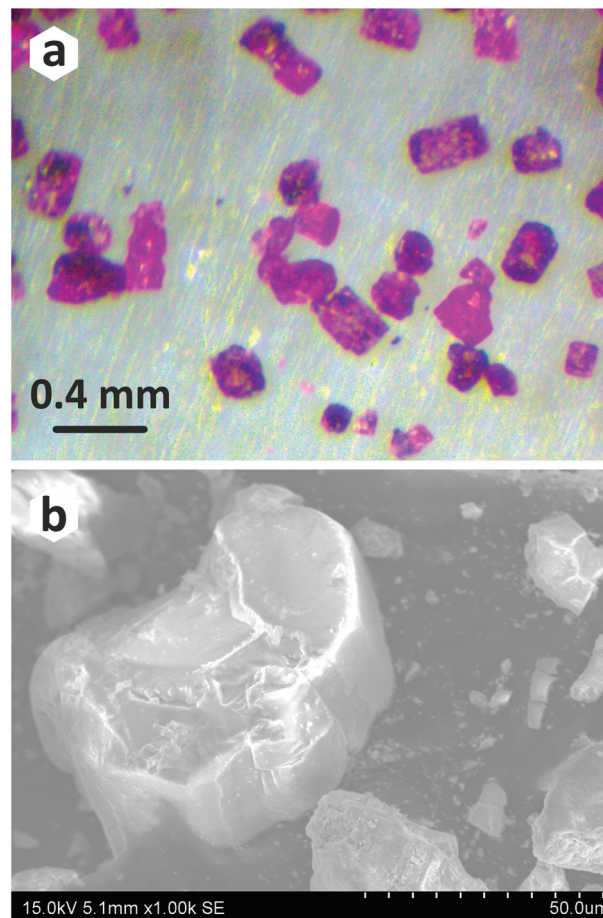
2.2 Single crystal X-ray diffraction studies

Single crystals of $PbCo_2(HPO_3)_3$ were mounted on thin glass fibers for X-ray diffraction (XRD) analysis and tested using a

Fig. 1 Optical (a) and scanning electron (b) microscope images of crystals of $PbCo_2(HPO_3)_3$. SEM images were obtained on a HITACHI S4700 microscope at 15 kV acceleration voltage and a current of 15 μA.

Bruker X8 APEX II X-ray diffractometer with a fine-focus X-ray tube delivering a MoKα radiation, $\lambda = 0.71073$ Å at 50 kV and 40 mA. More than a hemisphere of three-dimensional XRD data was collected with frame widths of 0.5° in ω, and a 30 s count time for each frame. The diffraction data were integrated and corrected for the absorption using a multi-scan type model integrated in the APEX2 and SADABS Bruker programs. The unit cell parameters of $PbCo_2(HPO_3)_3$ ($R3m$, $a = 5.3145(15)$ Å, $c = 25.494(7)$ Å, $V = 623.6(4)$ Å^3, $Z = 3$) were determined and refined by least-squares techniques on the basis of 3265 reflections with 2θ in the range between 4.8 and 63.48°. The crystal structure of $PbCo_2(HPO_3)_3$ was solved in the non-centrosymmetric $R3m$ space group by direct methods and refined to $R_1 = 0.015$ ($wR_2 = 0.030$) for 534 reflections with $|F_o| \geq 4\sigma F$ by using the SHELXL–2013 program implemented in the WinGX program package.[27] The final model included coordinates and anisotropic displacement parameters for all non-hydrogen atoms. The "ideal" hydrogen atoms of the $(HPO_3)^{2-}$ groups were localized from the difference Fourier maps. Data collection refinement parameters and detailed crystallographic information are provided in Table 2. Fractional atomic coordi-

Table 1 List of performed experiments in attempts to obtain a pure powder sample of new $PbCo_2(HPO_3)_3$

No.	Precursors (+6 ml H_2O)	Products	Ref.
1	PbO : Co_3O_4 : H_3PO_3 = 0.67 : 0.33 : 2.00	i. $PbCo_2(HPO_3)_3$ ii. $PbHPO_4$	*a* 22 and 23
2	PbO : Co_3O_4 : H_3PO_3 = 1.00 : 0.67 : 3.00	i. $PbCo_2(HPO_3)_3$ ii. $PbHPO_3$ iii. $Pb_3(PO_4)_2$	*a* 24 25 and 26
3	PbO : CoO : H_3PO_3 = 1.00 : 2.00 : 3.00	i. $PbCo_2(HPO_3)_3$ ii. $PbHPO_4$ iii. $PbHPO_3$	*a* 22 and 23 24

a This work.

Table 2 Crystallographic information and single crystal refinement parameters for $PbCo_2(HPO_3)_3$

Crystal data

Chemical formula	$PbCo_2(HPO_3)_3$
Formula weight (g)	564.98
Crystal system	Trigonal
Space group	$R3m$ (no. 160)
a (Å)	5.3145(15)
c (Å)	25.494(7)
V (Å^3)	623.6(4)
Z	3
ρ_{calc} (g cm^{-3})	4.514
Crystal size (mm)	$0.20 \times 0.15 \times 0.13$

Data collection

Diffractometer	Bruker X8 APEX II (CCD)
Radiation, λ (Å)	MoKα, 0.71073
μ (mm^{-1})	24.75
F (000)	768
θ range (°)	2.4–32.0
No. of measured reflections	3590
Total reflections (R_{int})	534 (0.029)
Unique reflections with $\|F_o\| \geq 4\sigma F$	534

Refinement[a]

Refinement method	Full-matrix least-squares on F^2
Weighting coefficients a, b	0.0063, 0
Data/restraints/parameters	534/4/41
R_1, wR_2 ($\|F_o\| \geq 4\sigma F$)	0.0147, 0.0298
R_1, wR_2 (all data)	0.0147, 0.0298
GoF	1.034
Largest diff. peak and hole (e Å^{-3})	1.485, −0.555

[a] $R_1 = \sum \|\|F_o\| - \|F_c\|\| / \sum \|F_o\|$; w$R_2 = \{\sum[w(F_o^2 - F_c^2)_2] / \sum[w(F_o^2)^2]\}^{1/2}$; GoF $= \{\sum[w(F_o^2 - F_c^2)] / (n - p)\}^{1/2}$, where n is the number of reflections, and p is the number of refined parameters.

nates, atomic displacement parameters, and selected bond distances are listed in Tables 3 and 4. CSD 433061 contains the supplementary crystallographic information for $PbCo_2(HPO_3)_3$. This data can be obtained from FIZ Karlsruhe, 76344 Eggenstein-Leopoldshafen, Germany, http://www.fiz-karlsruhe.de/.

2.3 Powder X-ray diffraction studies

The grown single crystals were crushed using an agate mortar and then used for the powder X-ray diffraction analysis performed at room temperature in the 2θ range of 10–60° with a

Table 3 Atomic coordinates, equivalent isotropic displacement parameters, and calculated partial charges of atoms in the crystal structure of $PbCo_2(HPO_3)_3$

Atom	Wyck.	x	y	z	$U_{iso}*/U_{eq}$	Charge $\pm q$
Pb1	$3a$	0	0	0.16209(2)	0.01761(10)	+0.74757
Co1	$3a$	0	0	0.28985(5)	0.0099(2)	+0.89371
Co2	$3a$	1/3	2/3	0.07026(5)	0.0096(3)	+0.92617
P1	$3a$	2/3	1/3	0.09927(11)	0.0098(5)	+0.39751
P2	$3a$	1/3	1/3	0.32927(9)	0.0089(4)	+0.43115
P3	$3a$	1/3	2/3	0.25226(11)	0.0086(5)	+0.43475
O1	$9b$	0.3478(10)	0.1739(5)	0.34537(15)	0.0137(8)	−0.41732
O2	$9b$	0.5100(5)	0.0199(9)	0.11827(17)	0.0185(9)	−0.40610
O3	$9b$	0.6523(9)	0.8262(5)	0.23647(15)	0.0147(9)	−0.40187
H1	$3a$	2/3	1/3	0.049(2)	0.022*	−0.05623
H2	$3a$	2/3	1/3	0.273(3)	0.022*	−0.03701
H3	$3a$	1/3	2/3	0.303(2)	0.022*	−0.06166

Table 4 Selected interatomic distances (Å) in the structure of $PbCo_2(HPO_3)_3$

Distance	Å	Distance	Å
Pb1–O3	$3 \times 2.481(4)$	P1–O2	$3 \times 1.522(4)$
Pb1–O2	$6 \times 2.8841(18)$	P2–O1	$3 \times 1.524(4)$
<Pb1–O>	2.6963	P3–O3	$3 \times 1.522(4)$
		<P–O>	1.523
Co1–O3	$3 \times 2.101(4)$		
Co1–O1	$3 \times 2.137(4)$	P1–H1	1.282(4)
Co2–O2	$3 \times 2.035(4)$	P2–H2	1.435(4)
Co2–O1	$3 \times 2.183(4)$	P3–H3	1.294(4)
<Co–O>	2.114	<P–H>	1.337(4)
Co1–Co2	2.900(2)	H1–H3	2.023(4)

scan step width of 0.02° using a D8 Advance Bruker AXS diffractometer (CuKα radiation, λ = 1.5418 Å). Difference of the XRD peak intensities between two patterns implies preferred orientation along [00l] as the XRD pattern was collected using crushed single crystals on a silicon crystal sample holder. A good coincidence between experimental and theoretical powder XRD patterns for the title compound is shown in Fig. 2.

2.4 IR spectroscopy

The infrared spectrum of $PbCo_2(HPO_3)_3$ was obtained between 4000 and 400 cm^{-1} with a PerkinElmer Spectrum Two spectrometer equipped with a diamond attenuated total reflectance (ATR) accessory. The vibrational bands of phosphite groups have been established in the studied range. Stretching vibrations and deformation modes of phosphite oxoanions in $PbCo_2(HPO_3)_3$ are divided between the following modes:
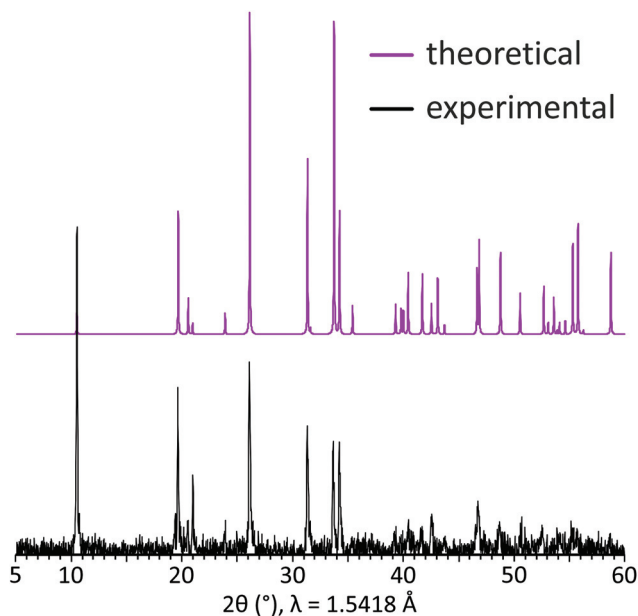
Fig. 2 Experimental (black) and theoretical (violet) powder XRD patterns for $PbCo_2(HPO_3)_3$.

ν(P–H): 2445 cm^{-1}, δ_{as}(P–H): 1030, 988 cm^{-1}; δ_s(P–O$_3$): 1065, 988 cm^{-1}, δ_s(P–O$_3$): 588–577, 554 cm^{-1}, δ_{as}(P–O$_3$): 477, 454 cm^{-1}. The presence of the typical P–H bond was preliminarily verified by infrared spectroscopy with evidence of the vibrational band at 2445 cm^{-1} (Fig. 3a). The observed values are similar to those found in other related compounds containing the phosphite ion.[6,28]
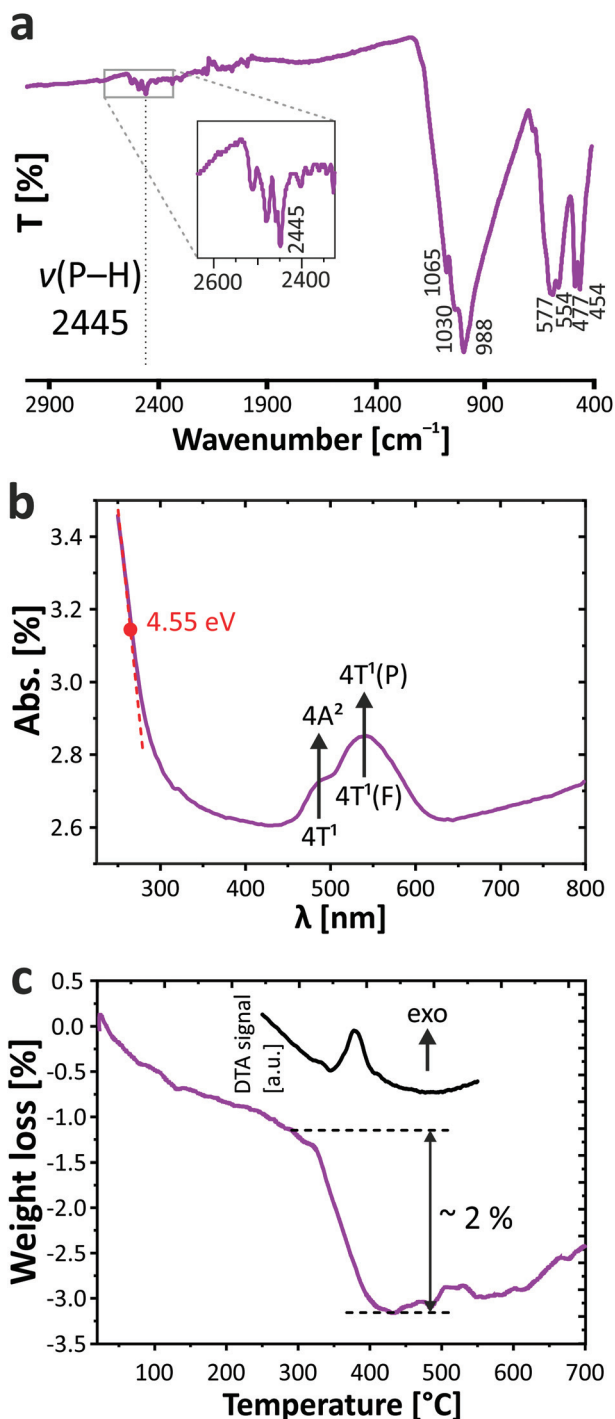

Fig. 3 IR- (a) and UV/vis spectra (b); TGA curve (c) for PbCo$_2$(HPO$_3$)$_3$.

2.5 UV/vis spectroscopy

The UV/vis absorbance spectrum was collected at room temperature with a PerkinElmer Lambda 650 spectrophotometer in the 250–800 nm range using an integration sphere designed for the characterization of solids. The spectrum is given in Fig. 3b. Beyond the band gap estimated at 4.55 eV of an insulating regime, it demonstrates the typical d–d transition of Co^{2+} in a high spin configuration. The main transition and the shoulder at lower energy are assigned to the 4T^1(F) to 4T^1(P) and 4T^1 to 4A^2 transitions. The resulting broad doublet between 450 and 600 nm (green to orange absorption) justifies the pink color of the crystal, *i.e.*, its complementary spectral color.

2.6 Thermogravimetric analysis

The thermogravimetric experiments have been carried out on a thermoanalyzer TGA 92 SETARAM under air atmosphere with a heating rate of 5 °C min^{-1} from room temperature up to 700 °C. The TGA curve (Fig. 3c) shows a constant weight loss assigned to moisture, while a sudden step occurs from both TGA and DTA at 380 °C, signing the phase decomposition. The corresponding loss of *ca.* 2% is hard to assign due to the poor crystalline residue after TGA. However as expected from the phosphite reactivity,[29] it most plausibly includes the removal of all H atoms with loss of water molecules (1.5 H$_2$O, *i.e.*, −4.7% mass loss) together with the partial oxidation by *ca.* one O atom (*i.e.*, 2.8% mass uptake), which is in good agreement with the experimental total weight loss of 2%. The latter is pursued at higher temperature with a constant mass increase and can be assigned to the oxidation of both the Co^{2+} and P^{3+} species. The final residue is black colored.

2.7 Magnetic measurements

The magnetic characterization of the new PbCo$_2$(HPO$_3$)$_3$ phase was performed on the crushed single crystals using a MPMS SQUID-VSM (Quantum Design) magnetometer in a temperature and field range of 1.8–400 K and 0–7 T, respectively. The temperature dependence of the magnetization was determined under various magnetic fields after cooling the sample in a field (FC, field cooling) or in a zero field (ZFC, zero-field cooling).

3. Results and discussion

3.1 Crystal structure

The new PbCo$_2$(HPO$_3$)$_3$ compound crystallizes in the *R*3*m* non-centrosymmetric space group. It is built up from alternating 2D layered blocks composed of (HPO$_3$)$^{2-}$ and (CoO$_6$)$^{10-}$ structural units separated by Pb^{2+} cations in the interlayer space (Fig. 4a). The crystal structure of PbCo$_2$(HPO$_3$)$_3$ contains two Co^{2+}, one Pb^{2+}, and three P^{3+} cations, which are crystallographically independent.

Both cobalt positions are located in the face-sharing octahedral dimers, with a Co⋯Co distance of 2.900 Å. The octahedral coordination of Co atoms is rather regular with the

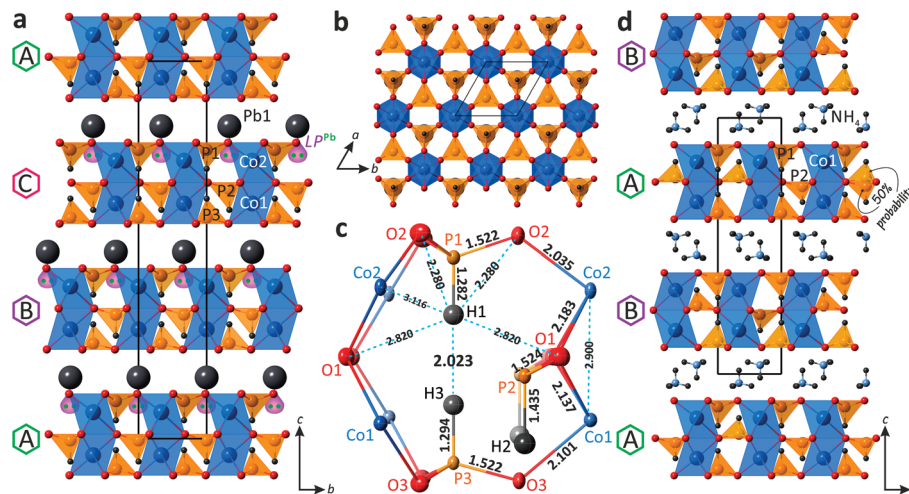**Fig. 4** General projections of the crystal structures of PbCo$_2$(HPO$_3$)$_3$ (a) and (NH$_4$)Co$_2$(HPO$_3$)$_3$ [30] (d) along the *a*-axis; [Co$_2$(HPO$_3$)$_3$]$^{2-}$ 2D block in PbCo$_2$(HPO$_3$)$_3$ projected on the *ab* plane (b); the atomic arrangement in the internal space of the 2D block (c).

average Co–O bond lengths of 2.118 Å and 2.109 Å for the Co1 and Co2 sites, respectively. The calculated bond valence sums give 1.89 and 1.98 v.u. (valence units) for Co1 and Co2, respectively, in good agreement with Co^{2+} species.

All three pseudo-tetrahedral HPO$_3$ oxoanions share all their O corners with adjacent cobalt octahedral dimers leading to 2D layered blocks in the *ab* plane (Fig. 4b). Thus, each phosphite pseudo-tetrahedron has three crystallographically identical P–O contacts (1.522 Å, 1.523 Å, and 1.522 Å for P1, P2, and P3, respectively) and a short hydrogen P–H bond (1.282 Å, 1.435 Å, and 1.294 Å for P1, P2, and P3, respectively). Note also the too short P1–H1 and P3–H3 bond lengths (≈ 1.29 Å) compared to the P2–H2 (≈ 1.44 Å) and the short H1···H3 contact of 2.023 Å, as a result of the orientation of the HP1O$_3$ and HP3O$_3$ pseudo-tetrahedra toward each other inside the 2D blocks, which may lead to local twisting of these polyhedra. The latter suggested resolving the crystal structure with off-centered one third occupied H sites (see below). The atomic arrangement in the internal space of the 2D block is demonstrated in Fig. 4c.

In the crystal structure of PbCo$_2$(HPO$_3$)$_3$, the unique Pb^{2+} cation adopts an irregular coordination with three equivalent short Pb–O bonds (2.481 Å) in the first coordination sphere and six identical longer bonds (2.884 Å) in the second coordination sphere. The observed asymmetric environment of the Pb polyhedra clearly indicates that the 6s^2 lone pair is stereochemically active (Fig. 4a). Divalent lead cations reside in the interlayer space of the structure and balance the charge of the negatively charged 2D blocks of the title compound. The non-centrosymmetric symmetry results from the "down" only orientation of the HP2O$_3$ groups in the crystal structure.

Similar 2D blocks have been reported in the crystal structure of (NH$_4$)$_2$Co$_2$(HPO$_3$)$_3$.[30] The main difference between these two compounds lies in the packing sequence of the 2D blocks and interlayer species between them, *i.e.*, double layers of NH$_4^+$ ions in (NH$_4$)$_2$Co$_2$(HPO$_3$)$_3$ and single layers of Pb^{2+} in PbCo$_2$(HPO$_3$)$_3$ (Fig. 4d). The most interesting structural feature

of the (NH$_4$)$_2$Co$_2$(HPO$_3$)$_3$ phase is the HP2O$_3$ site, which is split into two half-occupied positions located above or below the mirror plane of the 2D blocks in the centrosymmetric $P\bar{3}1c$ space group. Clearly, in the title compound the cooperative displacement of the lone pair on Pb^{2+} cations between the layers leads to the unique orientation of HP2O$_3$ in a non-centrosymmetric mode. We also note too-short H···H contacts (1.85 Å) in the blocks of (NH$_4$)$_2$Co$_2$(HPO$_3$)$_3$, but this observation was not commented on in the original publication.

The determination of partial charges using scales of atomic non-empirical electronegativity and hardness was carried out using Henry's method.[31,32] The average negative charge of −0.052 was found for the H atoms in PbCo$_2$(HPO$_3$)$_3$ (Table 3), which clearly indicates the hydride character of the terminal H in phosphite anions. The latter lies in accordance with an observed weak P$^{\delta+}$–H$^{\delta-}$ polarization in various inorganic phases containing (HPO$_3$)$^{2-}$ groups as reported in ref. 6.

3.2 Structural model with 1/3 occupied off-centered H sites

As mentioned in the previous section, inside the 2D blocks of the structure of PbCo$_2$(HPO$_3$)$_3$, two crystallographically inequivalent phosphite groups point toward each other leading to the unreasonably short H1···H3 = 2.023 Å, as refined in the *R*3*m* space-group symmetry. Note that it is close to the H···H contact in the PH$_3$ phosphorous trihydride, *i.e.*, H···H = 2.07 Å,[33] but significantly shorter than the sums of the van der Waals radii of H atoms. This abnormally short contact between two HPO$_3$ groups most plausibly denotes local off-centering of the H1 and H3 positions out of their ideal special 3*a* positions. The model of splitting of H1 and H3 into plausible *x*, 2*x*, and *z* positions (1/3rd occupied, see Fig. 5a) did not converge. However, the large thermal parameters of the coordinating oxygen atoms suggest local tilting around the *c*-axis to preserve the rigid HPO$_3$ configuration, as depicted in Fig. 5b and c. Similar features are observed in (NH$_4$)Co$_2$(HPO$_3$)$_3$,[30] which suggests the occurrence of similar local disorder.
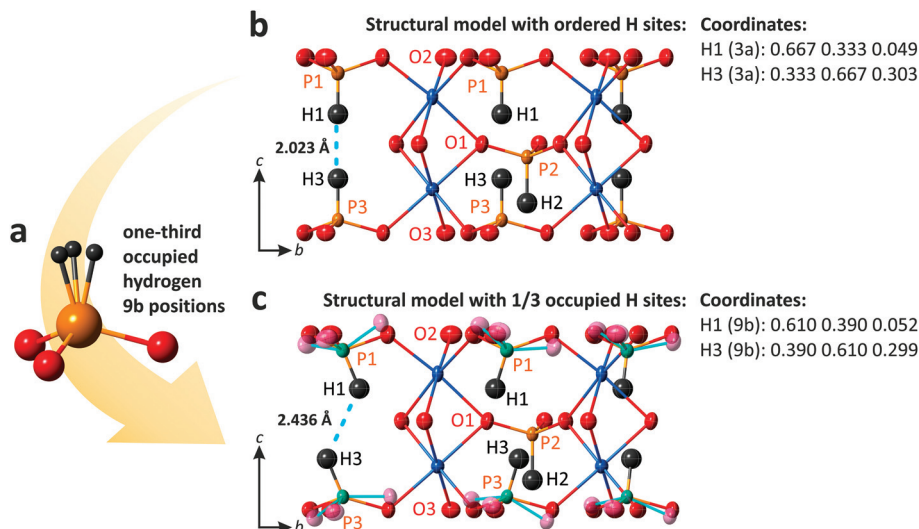
Fig. 5 HPO_3 group with one-third occupied hydrogen sites (a); structural models of $PbCo_2(HPO_3)_3$ with ordered (b) and one-third occupied H sites with tilting phosphite groups shown by a cyan color (c). Displacement ellipsoids are drawn at the 80% probability level.

For instance, setting H1 and H3 on the 9b sites (H1: 0.61, 0.39, 0.052 and H3: 0.39, 0.61, 0.299), one may get a reasonable length of 2.436 Å for the H···H contacts and P–H distances of 1.332 Å and 1.330 Å for P1 and P3, respectively.

3.3 Magnetic properties

One of the characteristics of phosphite $(HPO_3)^{2-}$ groups acting as ligands between transition metal ions is the strong tendency towards weak magnetic exchanges which denotes a poor ability for magnetic connections compared to standard tetrahedral ligands such as phosphate $(PO_4)^{3-}$ groups, despite similar P–O bond distances and P–O–P angles. Especially, it was shown in several compounds that the phosphite μ-O bridge between two metal centers gives rise to very weak exchanges, even for dimeric units with short Co···Co distances.[14] In $Fe_2(HPO_3)_3$ with face-sharing Fe dimers similar to those in the title compound, i.e., three μ_2-η^1 bridging modes (which mean three M–O–M paths with one single oxygen bridging two metal atoms in each) that the intra-dimer exchanges are ten times weaker than the inter-dimer exchanges.[6]

It mostly leads to extended Curie–Weiss (CW) thermal regimes down to low temperature in the absence of long-range magnetic ordering above 10 K. For instance, the behaviors reported for $A^I[M^{III}(HPO_3)_2]$ (A = K, NH_4, Rb; M = V, Fe)[28] show smooth deviation from the CW law, and Néel temperatures occur only for Fe^{3+} (S = 5/2) phases below T_N = 9 K at maximum.

For the new $PbCo_2(HPO_3)_3$ compound, the system obeys a Curie–Weiss law $\chi = C/(T - \theta_{CW})$ (C = 7.01 emu K Oe^{-1}; μ_{eff} = 7.48μ_B per FU; θ_{CW} = −69.4 K) down to 22 K which suggests weak spin exchanges. The magnetic susceptibility data for $PbCo_2(HPO_3)_3$ are provided in Fig. 6. The effective moment reflects a strong spin orbit coupling as expected for anisotropic Co^{2+} ions, i.e., the rough approximation $\mu_{eff} = g\sqrt{[S(S + 1)]}$

gives g = 2.73 instead of 2 for a spin-only contribution. It was not possible to fit χ using the analytical expression for dinuclear Co^{2+} (S = 3/2) compounds due to the strong spin–orbit interaction and other parameters inherent to high spin Co^{2+},[34] even after correction from a temperature independent term describing a residual paramagnetic contribution (see ref. 35). Once again, the structural analogy of the magnetic M–O–M paths with those found in $Fe_2(HPO_3)_3$[6] suggests very weak intra-dimer exchanges, in good agreement with the $\chi(T)$ shape with smooth deviations from the Curie–Weiss law. The magnetic exchange coupling can be roughly estimated using the mean-field approximation:

$$J/k_B = 3\theta_{CW}/[2zS(S + 1)] = -69 \text{ K},$$

where S = 3/2 and z is the number of neighboring Co^{2+} ions, i.e. z = 1 intra-dimer + 6 inter-dimer. Thus, we find J/k_B = −3.9 K.

The bi-exponential phenomenological equation given below can be used to describe the $\chi T(T)$ product for the interplay of two thermally activated phenomena (Fig. 6c), for instance weak AFM occurrence in an antiferromagnetic matrix:[35,36]

$$\chi T = A \exp(-E_1/kT) + B \exp(-E_2/kT),$$

where A + B equals the Curie constant. In Co^{2+} low-D systems it adequately describes thermally activated splitting between discrete levels (spin–orbit coupling) and the exponential temperature divergence of χ (antiferromagnetic exchange).[35–38] We find A = 1.88(1), E_1/k_B = 3.64(5) K very similar to the weak 3D antiferromagnetic exchange deduced from the Weiss constant and B = 4.68(1), E_2/k_B = 68.9(5) K in full agreement with values (ca. 100 K) reported for the activation of the spin–orbit coupling effect and site distortion.[39] Furthermore, the sum A + B (= 6.56) is in excellent agreement with the fitted Curie constant of 7.01 emu K/Oe per unit formula expected for two Co^{2+} ions. Finally, at 1.8 K the $\chi(T)$ anomaly suggests a Néel AFM order-

a PbCo$_2$(HPO$_3$)$_3$
μ_{eff} = 7.5 μ_B/FU
θ_{CW} = −69 K

Inset: FC 200 Oe, ZFC 200 Oe

b M [μ_B/Co^{2+}] vs H [kOe]
T = 1.8 K
T = 5 K
T = 15 K
T = 100K
T = 300 K

c $\chi \cdot T$ [emu·K·Oe^{-1}·mol^{-1}] vs Temperature [K]
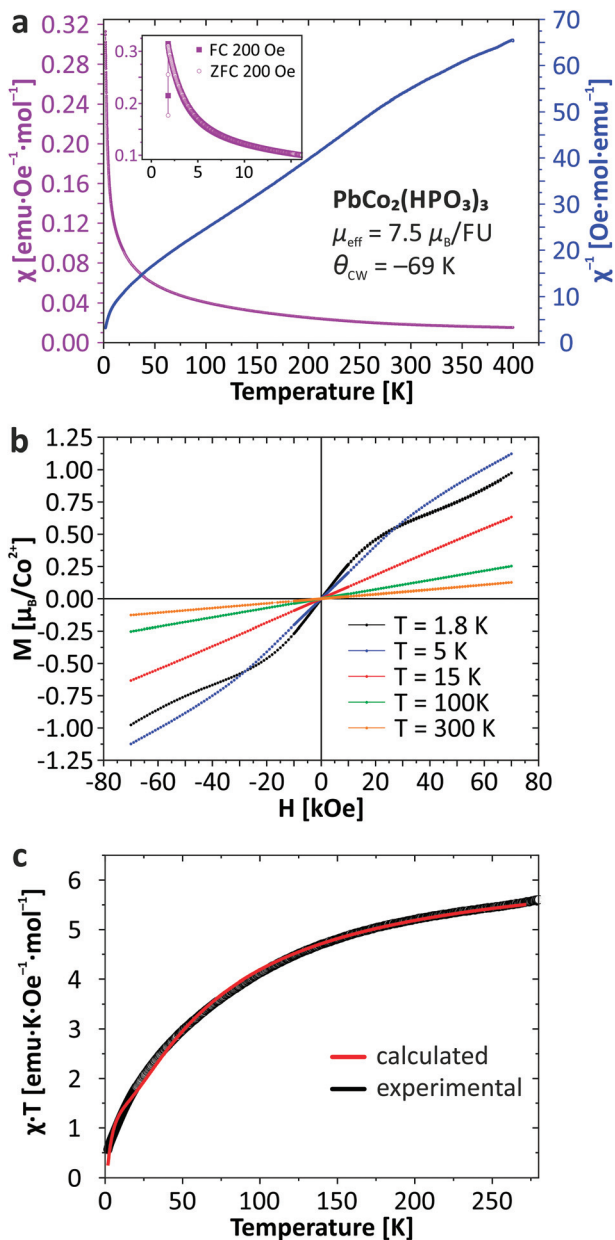calculated
experimental

Fig. 6 Thermal evolution of the magnetic susceptibility (a); magnetization as a function of applied field (b), and temperature dependence of χT (c) for PbCo$_2$(HPO$_3$)$_3$.

ing. This low T_N value validates the very small strength of this interaction.

4. Conclusion

The first lead cobalt phosphite PbCo$_2$(HPO$_3$)$_3$ has been prepared using mild hydrothermal techniques. Its non-centrosymmetric crystal structure is consistent with the stereoactive lone-pair effect of Pb^{2+} ions arranged cooperatively in the structure. It is built up from alternating 2D blocks composed of Co$_2$O$_9$ dimers and HPO$_3$ groups, which share common O

corners. Divalent lead cations with stereochemically active lone electron pairs reside in the interlayer space between the 2D blocks and balance the charge. Similar blocks have been observed in the centrosymmetric structure of (NH$_4$) Co$_2$(HPO$_3$)$_3$,[30] which is distinguished from the title compound by a different sequence of stacking of the layered cobalt phosphite blocks. Another structural feature of PbCo$_2$(HPO$_3$)$_3$ is the evidence of an unreasonably short H⋯H contact (2.02 Å) between two HPO$_3$ groups oriented toward each other inside the 2D block. A local twisting of the HPO$_3$ oxoanions and off-centering of the H sites around the average special position with 1/3rd occupancy may give a more reasonable distance of 2.44 Å for the H⋯H contacts. The measurement of the magnetic properties of PbCo$_2$(HPO$_3$)$_3$ reveals weak antiferromagnetic interactions between the cobalt ions inside the Co$_2$O$_9$ dimers due to the weak μ-O magnetic connectors with the bridging oxygen part of the phosphite groups. This aspect reinforces the interest of phosphite ligands as strong diamagnetic spacers ideally residing between compact metal center clusters.

Conflicts of interest

There are no conflicts to declare.

Acknowledgements

References

1 M. Plabst, L. B. McCusker and T. Bein, *J. Am. Chem. Soc.*, 2009, **131**, 18112–18118.
2 S. Natarajan and S. Mandal, *Angew. Chem., Int. Ed. Engl.*, 2008, **47**, 4798–4828.

3 T. Rojo, J. L. Mesa, J. Lago, B. Bazan, J. L. Pizarro and M. I. Arriortua, *J. Mater. Chem.*, 2009, **19**, 3793.

4 C. Y. Ortiz-Avila, P. J. Squattrito, M. Shieh and A. Clearfield, *Inorg. Chem.*, 1989, **28**, 2608–2615.

5 M. Shieh, K. J. Martin, P. J. Squattrito and A. Clearfield, *Inorg. Chem.*, 1990, **29**, 958–963.

6 V. M. Kovrugin, E. E. Gordon, E. E. Kasapbasi, M.-H. Whangbo, M. Colmont, O. I. Siidra, S. Colis, S. V. Krivovichev and O. Mentré, *J. Phys. Chem. C*, 2016, **120**, 1650–1656.

7 V. M. Kovrugin, M. Colmont, O. I. Siidra, S. V. Krivovichev and O. Mentré, *Cryst. Growth Des.*, 2016, **16**, 3113–3123.

8 X.-L. Cao, F. Kong, C.-L. Hu, X. Xu and J.-G. Mao, *Inorg. Chem.*, 2014, **53**, 8816–8824.

9 A. Aliev, V. M. Kovrugin, M. Colmont, C. Terryn, M. Huvé, O. I. Siidra, S. V. Krivovichev and O. Mentré, *Cryst. Growth Des.*, 2014, **14**, 3026–3034.

10 V. M. Kovrugin, M. Colmont, C. Terryn, S. Colis, O. I. Siidra, S. V. Krivovichev and O. Mentré, *Inorg. Chem.*, 2015, **54**, 2425–2434.

11 X. Liu, Y. Xing, X. Wang, H. Xu, X. Liu, K. Shao and Z. Su, *Chem. Commun.*, 2010, **46**, 2614.

12 A. Baiker, *Curr. Opin. Solid State Mater. Sci.*, 1998, **3**, 86–93.

13 S. Zheng, X. Li, B. Yan, Q. Hu, Y. Xu, X. Xiao, H. Xue and H. Pang, *Adv. Energy Mater.*, 2017, 1602733.

14 J. Fan, G. T. Yee, G. Wang and B. E. Hanson, *Inorg. Chem.*, 2006, **45**, 599–608.

15 X. Liu, Y. Xing and X. Liu, *CrystEngComm*, 2010, **12**, 383–386.

16 X.-M. Jing, Y.-B. Tan, L.-W. Xiao and Y.-L. Liu, *Inorg. Chem. Commun.*, 2015, **57**, 75–77.

17 J. Zhang, Z. Yao, S. Liao, J. Dai and Z. Fu, *J. Mater. Chem. A*, 2013, **1**, 4945–4948.

18 B. Kratochvíl, J. Podlahová, S. Habibpur, V. Petříček and K. Malý, *Acta Crystallogr., Sect. B: Struct. Crystallogr. Cryst. Chem.*, 1982, **38**, 2436–2438.

19 F. Sapiña, P. Gómez-Romero, M. D. Marcos, P. Amorós, R. Ibanez and D. Beltrán-Porter, *Eur. J. Solid State Inorg. Chem.*, 1989, **26**, 603–617.

20 M. D. Marcos, P. Amorós, A. Beltrán-Porter, R. Martinez-Manez and J. P. Attfield, *Chem. Mater.*, 1993, **5**, 121–128.

21 W. Liu, H.-H. Chen, X.-X. Yang and J.-T. Zhao, *Eur. J. Inorg. Chem.*, 2005, **2005**, 946–951.

22 H. Effenberger and F. Pertlik, *TMPM, Tschermaks Mineral. Petrogr. Mitt.*, 1986, **35**, 157–166.

23 A. Katrusiak and R. J. Nelmes, *J. Phys.: Condens. Matter*, 1989, **1**, 10165–10174.

24 B. Liu, D. Li and C. Che, *Rare Met. Mater. Eng.*, 2003, **32**, 862–865.

25 U. Keppler, *Z. Kristallogr. - Cryst. Mater.*, 1970, **132**, 228–235.

26 H. N. Ng and C. Calvo, *Can. J. Phys.*, 1975, **53**, 42–51.

27 G. M. Sheldrick, *Acta Crystallogr., Sect. C: Cryst. Struct. Commun.*, 2015, **71**, 3–8.

28 F. Hamchaoui, V. Alonzo, D. Venegas-Yazigi, H. Rebbah and E. Le Fur, *J. Solid State Chem.*, 2013, **198**, 295–302.

29 H. Y. Asl, K. Ghosh, M. P. Vidal Meza and A. Choudhury, *J. Mater. Chem. A*, 2015, **3**, 7488–7497.

30 C.-C. Cheng, W.-K. Chang, R.-K. Chiang and S.-L. Wang, *J. Solid State Chem.*, 2010, **183**, 304–309.

31 M. Henry, *ChemPhysChem*, 2002, **3**, 561–569.

32 M. Henry, in *Advances in quantum chemical bonding structures*, ed. M. V. Putz, Transworld Research Network, Kerala, India, 2008, pp. 153–211.

33 T. Shimanouchi, I. Nakagawa, J. Hiraishi and M. Ishii, *J. Mol. Spectrosc.*, 1966, **19**, 78–107.

34 Z. Tomkowicz, S. Ostrovsky, S. Foro, V. Calvo-Perez and W. Haase, *Inorg. Chem.*, 2012, **51**, 6046–6055.

35 L. Cui, G.-P. Yang, W.-P. Wu, H.-H. Miao, Q.-Z. Shi and Y.-Y. Wang, *Dalton Trans.*, 2014, **43**, 5823–5830.

36 X.-Y. Wang and S. C. Sevov, *Inorg. Chem.*, 2008, **47**, 1037–1043.

37 J.-M. Rueff, N. Masciocchi, P. Rabu, A. Sironi and A. Skoulios, *Eur. J. Inorg. Chem.*, 2001, **2001**, 2843–2848.

38 L.-L. Liang, S.-B. Ren, J. Wang, J. Zhang, Y.-Z. Li, H.-B. Du and X.-Z. You, *CrystEngComm*, 2010, **12**, 2669–2671.

39 R. L. Carlin, *Magnetochemistry*, Springer-Verlag, Berlin, Heidelberg, 1986.